

An Improved Measurement of Neutrino Oscillation Parameters by the NOvA Experiment

M. A. Acero,² P. Adamson,¹² L. Aliaga,¹² N. Anfimov,²⁶ A. Antoshkin,²⁶ E. Arrieta-Diaz,²⁸ L. Asquith,⁴¹ A. Aurisano,⁶ A. Back,^{20,24} C. Backhouse,⁴⁵ M. Baird,^{20,41,46} N. Balashov,²⁶ P. Baldi,²⁵ B. A. Bambah,¹⁷ S. Bashar,⁴⁴ K. Bays,^{4,19} R. Bernstein,¹² V. Bhatnagar,³⁴ D. Bhattarai,³² B. Bhuyan,¹⁴ J. Bian,^{25,31} J. Blair,¹⁶ A. C. Booth,⁴¹ R. Bowles,²⁰ C. Bromberg,²⁹ N. Buchanan,⁸ A. Butkevich,²² S. Calvez,⁸ T. J. Carroll,^{43,49} E. Catano-Mur,⁴⁸ B. C. Choudhary,¹⁰ A. Christensen,⁸ T. E. Coan,³⁹ M. Colo,⁴⁸ L. Cremonesi,^{36,45} G. S. Davies,^{32,20} P. F. Derwent,¹² P. Ding,¹² Z. Djurcic,¹ M. Dolce,⁴⁴ D. Doyle,⁸ D. Dueñas Tonguino,⁶ E. C. Dukes,⁴⁶ H. Duyang,³⁸ R. Ehrlich,⁴⁶ M. Elkins,²⁴ E. Ewart,²⁰ G. J. Feldman,¹⁵ P. Filip,²³ J. Franc,⁹ M. J. Frank,³⁷ H. R. Gallagher,⁴⁴ R. Gandrajula,^{29,46} F. Gao,³⁵ A. Giri,¹⁸ R. A. Gomes,¹³ M. C. Goodman,¹ V. Grichine,²⁷ M. Groh,^{8,20} R. Group,⁴⁶ B. Guo,³⁸ A. Habig,³⁰ F. Hakl,²¹ A. Hall,⁴⁶ J. Hartnell,⁴¹ R. Hatcher,¹² H. Hausner,⁴⁹ M. He,¹⁶ K. Heller,³¹ V. Hewes,⁶ A. Himmel,¹² A. Holin,⁴⁵ J. Huang,⁴³ B. Jargowsky,²⁵ J. Jarosz,⁸ F. Jedyň,⁹ C. Johnson,⁸ M. Judah,^{8,35} I. Kakorin,²⁶ D. M. Kaplan,¹⁹ A. Kalitkina,²⁶ R. Keloth,⁷ O. Klimov,²⁶ L. W. Koerner,¹⁶ L. Kolupaeva,²⁶ S. Kotelnikov,²⁷ R. Kralik,⁴¹ Ch. Kullenberg,²⁶ M. Kubu,⁹ A. Kumar,³⁴ C. D. Kuruppu,³⁸ V. Kus,⁹ T. Lackey,²⁰ K. Lang,⁴³ P. Lasorak,⁴¹ J. Lesmeister,¹⁶ S. Lin,⁸ A. Lister,⁴⁹ J. Liu,²⁵ M. Lokajicek,²³ S. Magill,¹ M. Manrique Plata,²⁰ W. A. Mann,⁴⁴ M. L. Marshak,³¹ M. Martinez-Casales,²⁴ V. Matveev,²² B. Mayes,⁴¹ D. P. Méndez,⁴¹ M. D. Messier,²⁰ H. Meyer,⁴⁷ T. Miao,¹² W. H. Miller,³¹ S. R. Mishra,³⁸ A. Mislivec,³¹ R. Mohanta,¹⁷ A. Moren,³⁰ A. Morozova,²⁶ W. Mu,¹² L. Muallem,⁴ M. Muether,⁴⁷ S. Mufson,²⁰ K. Mulder,⁴⁵ D. Naples,³⁵ N. Nayak,²⁵ J. K. Nelson,⁴⁸ R. Nichol,⁴⁵ E. Niner,¹² A. Norman,¹² A. Norrick,¹² T. Nosek,⁵ H. Oh,⁶ A. Olshevskiy,²⁶ T. Olson,⁴⁴ J. Ott,²⁵ J. Paley,¹² R. B. Patterson,⁴ G. Pawloski,³¹ O. Petrova,²⁶ R. Petti,³⁸ D. D. Phan,^{43,45} R. K. Plunkett,¹² J. C. C. Porter,⁴¹ A. Rafique,¹ F. Psihas,^{20,43} V. Raj,⁴ M. Rajaoalisoa,⁶ B. Ramson,¹² B. Rebel,^{12,49} P. Rojas,⁸ P. Roy,⁴⁷ V. Ryabov,²⁷ O. Samoylov,²⁶ M. C. Sanchez,²⁴ S. Sánchez Falero,²⁴ P. Shanahan,¹² A. Sheshukov,²⁶ P. Singh,¹⁰ V. Singh,³ E. Smith,²⁰ J. Smolik,⁹ P. Snopok,¹⁹ N. Solomey,⁴⁷ A. Sousa,⁶ K. Soustruznik,⁵ M. Strait,³¹ L. Suter,¹² A. Sutton,⁴⁶ S. Swain,³³ C. Sweeney,⁴⁵ A. Sztuc,⁴⁵ R. L. Talaga,¹ B. Tapia Oregui,⁴³ P. Tas,⁵ T. Thakore,⁶ R. B. Thayyullathil,⁷ J. Thomas,^{45,49} E. Tiras,^{11,24} J. Tripathi,³⁴ J. Trokan-Tenorio,⁴⁸ A. Tsaris,¹² Y. Torun,¹⁹ J. Urheim,²⁰ P. Vahle,⁴⁸ Z. Vallari,⁴ J. Vasel,²⁰ P. Vokac,⁹ T. Vrba,⁹ M. Wallbank,⁶ T. K. Warburton,²⁴ M. Wetstein,²⁴ D. Whittington,^{42,20} D. A. Wickremasinghe,¹² S. G. Wojcicki,⁴⁰ J. Wolcott,⁴⁴ W. Wu,²⁵ Y. Xiao,²⁵ A. Yallappa Dombara,⁴² A. Yankelevich,²⁵ K. Yonehara,¹² S. Yu,^{1,19} Y. Yu,¹⁹ S. Zadorozhnyy,²² J. Zalesak,²³ Y. Zhang,⁴¹ and R. Zwaska¹²

(The NOvA Collaboration)

¹Argonne National Laboratory, Argonne, Illinois 60439, USA

²Universidad del Atlantico, Carrera 30 No. 8-49, Puerto Colombia, Atlantico, Colombia

³Department of Physics, Institute of Science, Banaras Hindu University, Varanasi, 221 005, India

⁴California Institute of Technology, Pasadena, California 91125, USA

⁵Charles University, Faculty of Mathematics and Physics, Institute of Particle and Nuclear Physics, Prague, Czech Republic

⁶Department of Physics, University of Cincinnati, Cincinnati, Ohio 45221, USA

⁷Department of Physics, Cochin University of Science and Technology, Kochi 682 022, India

⁸Department of Physics, Colorado State University, Fort Collins, CO 80523-1875, USA

⁹Czech Technical University in Prague, Břehova 7, 115 19 Prague 1, Czech Republic

¹⁰Department of Physics and Astrophysics, University of Delhi, Delhi 110007, India

¹¹Department of Physics, Erciyes University, Kayseri 38030, Turkey

¹²Fermi National Accelerator Laboratory, Batavia, Illinois 60510, USA

¹³Instituto de Física, Universidade Federal de Goiás, Goiânia, Goiás, 74690-900, Brazil

¹⁴Department of Physics, IIT Guwahati, Guwahati, 781 039, India

¹⁵Department of Physics, Harvard University, Cambridge, Massachusetts 02138, USA

¹⁶Department of Physics, University of Houston, Houston, Texas 77204, USA

¹⁷School of Physics, University of Hyderabad, Hyderabad, 500 046, India

¹⁸Department of Physics, IIT Hyderabad, Hyderabad, 502 205, India

¹⁹Illinois Institute of Technology, Chicago IL 60616, USA

²⁰Indiana University, Bloomington, Indiana 47405, USA

²¹Institute of Computer Science, The Czech Academy of Sciences, 182 07 Prague, Czech Republic

²²Institute for Nuclear Research of Russia, Academy of Sciences 7a, 60th October Anniversary prospect, Moscow 117312, Russia

²³Institute of Physics, The Czech Academy of Sciences, 182 21 Prague, Czech Republic

²⁴Department of Physics and Astronomy, Iowa State University, Ames, Iowa 50011, USA

²⁵Department of Physics and Astronomy, University of California at Irvine, Irvine, California 92697, USA

²⁶Joint Institute for Nuclear Research, Dubna, Moscow region 141980, Russia

- ²⁷ *Nuclear Physics and Astrophysics Division, Lebedev Physical Institute, Leninsky Prospect 53, 119991 Moscow, Russia*
²⁸ *Universidad del Magdalena, Carrera 32 No 22-08 Santa Marta, Colombia*
²⁹ *Department of Physics and Astronomy, Michigan State University, East Lansing, Michigan 48824, USA*
³⁰ *Department of Physics and Astronomy, University of Minnesota Duluth, Duluth, Minnesota 55812, USA*
³¹ *School of Physics and Astronomy, University of Minnesota Twin Cities, Minneapolis, Minnesota 55455, USA*
³² *University of Mississippi, University, Mississippi 38677, USA*
³³ *National Institute of Science Education and Research, Khurda, 752050, Odisha, India*
³⁴ *Department of Physics, Panjab University, Chandigarh, 160 014, India*
³⁵ *Department of Physics, University of Pittsburgh, Pittsburgh, Pennsylvania 15260, USA*
³⁶ *School of Physics and Astronomy, Queen Mary University of London, London E1 4NS, United Kingdom*
³⁷ *Department of Physics, University of South Alabama, Mobile, Alabama 36688, USA*
³⁸ *Department of Physics and Astronomy, University of South Carolina, Columbia, South Carolina 29208, USA*
³⁹ *Department of Physics, Southern Methodist University, Dallas, Texas 75275, USA*
⁴⁰ *Department of Physics, Stanford University, Stanford, California 94305, USA*
⁴¹ *Department of Physics and Astronomy, University of Sussex, Falmer, Brighton BN1 9QH, United Kingdom*
⁴² *Department of Physics, Syracuse University, Syracuse NY 13210, USA*
⁴³ *Department of Physics, University of Texas at Austin, Austin, Texas 78712, USA*
⁴⁴ *Department of Physics and Astronomy, Tufts University, Medford, Massachusetts 02155, USA*
⁴⁵ *Physics and Astronomy Department, University College London, Gower Street, London WC1E 6BT, United Kingdom*
⁴⁶ *Department of Physics, University of Virginia, Charlottesville, Virginia 22904, USA*
⁴⁷ *Department of Mathematics, Statistics, and Physics, Wichita State University, Wichita, Kansas 67206, USA*
⁴⁸ *Department of Physics, William & Mary, Williamsburg, Virginia 23187, USA*
⁴⁹ *Department of Physics, University of Wisconsin-Madison, Madison, Wisconsin 53706, USA*

We present new $\nu_\mu \rightarrow \nu_e$, $\nu_\mu \rightarrow \nu_\mu$, $\bar{\nu}_\mu \rightarrow \bar{\nu}_e$, and $\bar{\nu}_\mu \rightarrow \bar{\nu}_\mu$ oscillation measurements by the NOvA experiment, with a 50% increase in neutrino-mode beam exposure over the previously reported results. The additional data, combined with previously published neutrino and antineutrino data, are all analyzed using improved techniques and simulations. A joint fit to the ν_e , ν_μ , $\bar{\nu}_e$, and $\bar{\nu}_\mu$ candidate samples within the 3-flavor neutrino oscillation framework continues to yield a best-fit point in the normal mass ordering and the upper octant of the θ_{23} mixing angle, with $\Delta m_{32}^2 = (2.41 \pm 0.07) \times 10^{-3} \text{ eV}^2$ and $\sin^2 \theta_{23} = 0.57^{+0.03}_{-0.04}$. The data disfavor combinations of oscillation parameters that give rise to a large asymmetry in the rates of ν_e and $\bar{\nu}_e$ appearance. This includes values of the CP-violating phase in the vicinity of $\delta_{\text{CP}} = \pi/2$ which are excluded by $> 3\sigma$ for the inverted mass ordering, and values around $\delta_{\text{CP}} = 3\pi/2$ in the normal ordering which are disfavored at 2σ confidence.

I. INTRODUCTION

We report new measurements of neutrino oscillation parameters using neutrino and antineutrino data from the NOvA experiment. The data include a 50% increase in neutrino-mode beam exposure over the previously reported results [1]. We perform a joint fit to ν_μ ($\bar{\nu}_\mu$) $\rightarrow \nu_e$ ($\bar{\nu}_e$) and ν_μ ($\bar{\nu}_\mu$) $\rightarrow \nu_\mu$ ($\bar{\nu}_\mu$) oscillations utilizing improvements in the analysis of these data.

Numerous experiments [2–10] corroborate the paradigm in which three neutrino mass eigenstates (ν_1, ν_2, ν_3) mix to form the three observable flavor eigenstates (ν_e, ν_μ, ν_τ). The mixing can be expressed by the unitary matrix, U_{PMNS} , named for Pontecorvo, Maki, Nakagawa, and Sakata. U_{PMNS} can be parameterized by three mixing angles ($\theta_{12}, \theta_{23}, \theta_{13}$) along with a phase (δ_{CP}) that, if nonzero, indicates violation of Charge-Parity (CP) symmetry. Neutrino mixing gives rise to oscillations from one flavor state to another, dependent on the oscillating parameters and the mass splittings ($\Delta m_{ij}^2 \equiv m_i^2 - m_j^2$).

Using the definition of ν_1 as having the largest ν_e contribution, it has been established that Δm_{21}^2 is positive, and therefore, the ν_2 mass eigenstate is heavier than ν_1 . However, the sign of the larger mass splitting, Δm_{32}^2 , is

unknown. If this term is positive, then the third mass eigenstate is the heaviest, and the mass ordering is labeled as the Normal Ordering (NO) (also referred to as Normal Hierarchy). The alternative is referred to as Inverted Ordering (IO). Knowing the mass ordering would constrain models of neutrino masses [11–15] and aid in the resolution of the Dirac or Majorana nature of the neutrino [16, 17].

The mass ordering affects the rates of $\nu_\mu \rightarrow \nu_e$ and $\bar{\nu}_\mu \rightarrow \bar{\nu}_e$ oscillations when neutrinos travel through the Earth as compared to a vacuum. Coherent forward scattering on electrons in the Earth’s crust enhances the rate of $\nu_\mu \rightarrow \nu_e$ oscillations and suppresses $\bar{\nu}_\mu \rightarrow \bar{\nu}_e$ for the NO while the enhancement and suppression is reversed for the IO. This matter effect [18] changes the oscillation probabilities for NOvA by $\sim 20\%$. Depending on the value of δ_{CP} and the mass ordering itself, NOvA may be able to exploit the resulting neutrino-antineutrino asymmetry to measure the sign of Δm_{32}^2 and thus determine the mass ordering.

The angle θ_{23} largely determines the coupling of the ν_μ and ν_τ states to the ν_3 mass state. In the case of maximal mixing, $\theta_{23} = \pi/4$, ν_μ and ν_τ couple equally to ν_3 [19], which suggests a $\mu - \tau$ symmetry. If non-maximal, θ_{23} could lie in the upper octant (UO, $\theta_{23} > \pi/4$) or lower

octant (LO, $\theta_{23} < \pi/4$) with a stronger ν_μ or ν_τ coupling, respectively. Current measurements of θ_{23} are near maximal mixing [1, 6, 7], but significant uncertainties remain making it the least precisely measured mixing angle.

NOvA also has sensitivity to δ_{CP} , which will increase the $\nu_\mu \rightarrow \nu_e$ oscillation probability if $\sin \delta_{\text{CP}}$ is positive and suppress oscillations if negative (the effect is reversed for antineutrinos). Additionally, a non-zero value of $\sin \delta_{\text{CP}}$ would identify the neutrino sector as a source of CP violation which is central to some explanations of the matter-antimatter asymmetry observed based on leptogenesis [20–24].

Here, we reanalyze the data taken in the antineutrino-mode beam from June 29, 2016, to February 26, 2019, with an exposure of 12.5×10^{20} protons on target (POT) delivered during 321.1 s of beam-on time. These data are combined with an increased, and reanalyzed, neutrino-mode beam exposure of 13.6×10^{20} POT from 555.3 s of beam-on time recorded between February 6, 2014, to March 20, 2020. During these periods, the proton source achieved an average power of 650 kW, and a peak hourly-averaged power of 756 kW.

In addition to the increased neutrino-mode beam exposure, this analysis introduces various improvements that will be described in detail in the following sections. There are changes to the underlying neutrino interaction simulation, particle propagation, and detector response models. The reconstruction uses a new initial clustering algorithm and expands the use of neural networks. Furthermore, the Near-to-Far extrapolation is now performed using an additional variable, reconstructed transverse momentum, that further constrains the FD predictions and reduces the impact of systematic uncertainties on the analysis by up to 9%. Finally, we have improved some systematic uncertainties and introduced new ones associated with the above changes.

II. THE NOvA EXPERIMENT AND SIMULATIONS

NOvA observes $\nu_\mu (\bar{\nu}_\mu) \rightarrow \nu_e (\bar{\nu}_e)$ appearance and $\nu_\mu (\bar{\nu}_\mu) \rightarrow \nu_\mu (\bar{\nu}_\mu)$ disappearance oscillations using two functionally-identical tracking calorimeters [25] deployed in the NuMI beam at Fermilab [26]. Charged particle tracking is accomplished via PVC cells filled with a mineral oil-based liquid scintillator [27]. The cells are 6.6 cm \times 3.9 cm in cross section and are oriented in alternating vertical and horizontal planes to achieve 3D reconstruction. The 290 ton Near Detector (ND) is located 100 m underground and \sim 1 km from the production target. The main body of the ND is followed by a muon range stack where the active planes are interleaved with steel plates. The 14 kton Far Detector (FD) is located at Ash River, MN, \sim 810 km from the source. Being located on the surface with a modest rock overburden, the FD receives a cosmic-ray flux of 130 kHz. This analysis benefits from an updated simulation of the geometries of the

detectors and their surroundings that more accurately reflects the surrounding rock composition and detectors as built.

Both detectors are centered 14.6 mrad off the beam axis and receive a narrow-band neutrino flux peaked at 1.8 GeV. Magnetic focusing horns are used to select the sign of the neutrino parents, producing a 93% (92%) pure $\nu_\mu (\bar{\nu}_\mu)$ beam between 1–5 GeV. The majority of contamination is due to “wrong-sign” neutrinos (*i.e.* $\bar{\nu}_\mu$ in a ν_μ selected beam and vice versa). The neutrino flux delivered to the detectors is calculated using GEANT4-based simulations of particle production and transport through the beamline components [26, 28] reweighted to incorporate external measurements using the Package to Predict the Flux (PPFX) [29–48].

Neutrino interactions are simulated using a custom model configuration of GENIE 3.0.6 [49, 50] tuned to external and NOvA ND data. This configuration uses models created by the València group [51, 52] for charged-current (CC) quasi-elastic (QE) scattering and interactions with two nucleons producing two holes (2p2h). The CCQE model includes the effects of long-range nucleon correlations calculated according to the Random Phase Approximation (RPA) [51, 53, 54]. The CCQE axial vector form factor is a z -expansion parameterization tuned to neutrino-deuterium scattering data [55]. A local Fermi gas represents the initial nuclear state in both the València QE and 2p2h models, while in all other processes the initial nuclear state is represented by a global relativistic Fermi gas with a high-momentum tail to account for short-range nucleon correlations [56]. Baryon resonance (RES) and coherent pion production are simulated using the Berger-Sehgal models with final-state mass effects taken into account [57, 58]. Deep inelastic scattering (DIS) and non-resonant background below the DIS region are described using the Bodek-Yang model [59] with hadronization simulated by a data-driven parameterization [60] coupled to PYTHIA [61]. RES, DIS, and non-resonant background processes are tuned by GENIE to free nucleon inclusive and exclusive 1- and 2-pion production CC neutrino scattering data. Final state interactions (FSI) are simulated by the GENIE hN semi-classical intranuclear cascade model in which pion interaction probabilities are assigned according to Oset *et al.* [62] and pion-nucleon scattering data.

The 2p2h and FSI models in this GENIE configuration are adjusted to produce a NOvA-specific neutrino interaction model tune. The 2p2h model is fit to ν_μ CC inclusive scattering data from the NOvA ND. Inspired by Gran *et al.* [63], this 2p2h tune enhances the base model as a function of energy and momentum transfer to the nucleus. The pion FSI parameters are changed to obtain agreement with π^+ on ^{12}C scattering data [64–70].

The propagation of final state particles through the detectors is simulated by an updated version of GEANT4 (v10.4) [71], which provides the input for the detector response simulation [72]. In addition, a custom patch to the new version implements an exact calculation us-

ing Sternheimer’s method [73] to calculate the density effect correction to the Bethe equation, compared to the approximate parameterization used previously.

The absolute energy scale for both detectors is calibrated using the minimum ionizing portion of stopping cosmic-ray muon tracks. The calibration procedure is now applied separately to the data in shorter time periods to account for an observed 0.3% decrease in detected light per year.

III. RECONSTRUCTION AND SELECTION

The first stage of reconstruction is to group hits, which are measurements of deposited energy in a cell above a preset threshold, into single-neutrino-interaction events. The initial grouping, performed based on hit proximity in time and space, is now performed with a new method that reduces the rate of mis-clustered hits in the high occupancy environment of the ND [74]. Mis-clustering had previously led to differences in data-MC selection efficiency. The other reconstruction techniques remain unchanged from the previous analysis [1].

For each event, initial selections are applied to ensure basic data quality. Additionally, events are required to be sufficiently far from the edges of the detector such that energy is not lost to exiting final-state particles, and entering background events are not selected as signal. These containment criteria have been re-optimized for this analysis due to changes in the geometry model and hit grouping algorithm, but follow the same outline as described in Ref. [1].

A convolutional neural network, CNN_{evt} [75], is used to classify neutrino event candidates into ν_e CC, ν_μ CC, NC, or cosmogenic background. The scores of CNN_{evt} are used to create two non-overlapping samples of either inclusive ν_μ ($\bar{\nu}_\mu$) CC or ν_e ($\bar{\nu}_e$) CC candidate events. Updates to this algorithm provide improved performance and decreased dependency on calorimetric energy, the dominant source of systematic uncertainty in the results presented here. To reduce the influence of calorimetric energy on classification decisions, a scale factor is applied to all pulse heights during network training. These scale factors are drawn on an event-by-event basis from a normal distribution with a 1σ range from 0.9-1.1 [76].

Effective rejection of cosmogenic backgrounds at the FD is paramount due to the significant flux of cosmic-ray particles it receives. A new CNN trained to identify and reject cosmogenic backgrounds has been introduced. This is utilized alongside boosted decision trees (BDTs), retrained on samples selected to contain signal-like cosmogenic particles. Together these selections reduce the cosmic contamination in the selected samples to $< 5\%$, a total reduction of 6 orders of magnitude, comparable to the previous analysis. For fully contained ν_e events, the BDT replaces the previous cosmic rejection method, which directly used reconstructed position and kinematic event information.

TABLE I. FD energy resolution and purity¹, in the selected energy ranges (0–5 GeV for ν_μ and 0–4 GeV for ν_e), for the subsamples used in the Near-to-Far extrapolation and oscillation fits. E_{frac} for the ν_μ samples is defined in the text. The ν_e ($\bar{\nu}_e$) peripheral is a rate-only sample, therefore, E_ν is not determined.

	Sample bins	Energy res.	Sample purity
ν_e ($\bar{\nu}_e$)	Core, Low CNN_{evt}	14.1% (13.7%)	51% (36%)
	Core, High CNN_{evt}	9.4% (8.9%)	79% (69%)
	Peripheral	–	57% (43%)
	Combined	10.7% (8.8%)	69% (58%)
ν_μ ($\bar{\nu}_\mu$)	1 (lowest E_{frac})	7.8% (8.5%)	99% (99%)
	2	9.2% (8.9%)	99% (99%)
	3	10.4% (9.7%)	97% (98%)
	4 (highest E_{frac})	11.5% (10.2%)	92% (95%)
	Combined	9.1% (8.2%)	96% (98%)

Neutrino energy, E_ν , is determined using different methods for the ν_e and ν_μ CC candidate events. The energy of ν_e CC candidates is estimated using a 2D quadratic fit to the electromagnetic (EM) and hadronic calorimetric energies. The EM and hadronic components produce different detector responses and are separated using a third CNN classifier that identifies EM-like hit clusters within the event [77]. For ν_μ CC candidates, E_ν is the sum of the muon track energy, determined by the track length, and the total calorimetric energy of the hadronic system, E_{had} . The muon is identified with a BDT that utilizes track length, multiple Coulomb scattering, and energy deposition, while the hadronic system is taken as all hits not associated with the muon track.

The selection criteria and energy estimation techniques were developed based on ND beam and FD cosmic data, along with simulated samples prior to inspecting the FD beam data distributions. The algorithms were trained separately on neutrino and antineutrino beam modes due to differences in beam purity and interactions.

The sensitivity of the oscillation fit is enhanced by splitting the fully contained ν_e and $\bar{\nu}_e$ CC, “core”, samples into low and high purity bins, based on the scores output by CNN_{evt} . At the FD, the ν_e ($\bar{\nu}_e$) selection efficiency for signal events in the core sample is 54% (64%)¹. To further increase the size of the FD sample, a “peripheral” selection is included, consisting of events that fail the containment or cosmic rejection requirements but pass more strict selection criteria on the cosmic BDT and CNN_{evt} . This sample increases the total ν_e ($\bar{\nu}_e$) selection efficiency to 63% (75%)¹ but is included only as an integrated rate in the oscillation fits due to possible energy

¹ The FD sample efficiency, purity, and energy resolution are based on the simulated event samples at the determined best-fit point. Wrong-sign events are treated as background for the ν_e ($\bar{\nu}_e$) CC samples and signal for the ν_μ ($\bar{\nu}_\mu$) CC samples. For the efficiency calculations, the denominator is the number of true signal interactions in the detector with no other selection criteria applied.

bias caused by particles leaving the detector. Properties of these subsamples are summarized in Table I.

For ν_μ CC candidates, the position and amplitude of the oscillation maximum in the FD energy spectra are strongly dependent on Δm_{32}^2 and θ_{23} , respectively. To maximize the sensitivity to these parameters, the candidates are divided into four equally populated samples based on the hadronic energy fraction, $E_{\text{frac}} = E_{\text{had}}/E_\nu$, which is correlated with energy resolution and background contamination as summarized in Table I. Sensitivity is further increased by using variably-sized E_ν bins for these samples.

IV. NEAR-TO-FAR EXTRAPOLATION

This analysis extracts oscillation parameters using data-driven predictions of the FD spectra largely derived from high statistics measurements in the ND. The ν_μ ($\bar{\nu}_\mu$) disappearance and ν_e ($\bar{\nu}_e$) appearance signal spectra in the FD are predicted using the spectra of ν_μ ($\bar{\nu}_\mu$) CC candidate events in the ND (Fig. 1a). The procedure begins with reweighting the simulation to obtain agreement with the data in each reconstructed E_ν bin of the ND ν_μ ($\bar{\nu}_\mu$) CC candidate samples. Predicted rates of NC, ν_e CC, and $\bar{\nu}_e$ CC interactions in the samples (<0.5% total) are taken directly from the simulation and subtracted. The wrong-sign component of the samples (2.9% and 10.5% in the neutrino and antineutrino beams respectively) is also taken directly from the simulation. The resulting corrected $\nu_\mu + \bar{\nu}_\mu$ CC reconstructed E_ν spectra are transformed to true E_ν using the simulation. The spectra are then multiplied by the appropriate far-to-near ratios of the simulated samples in bins of true E_ν . This step accounts for beam divergence, differences in selection efficiency and acceptance between the two detectors, and the differences in the ν_μ and ν_e cross sections. Oscillation probabilities are applied to yield the predicted disappearance or appearance signal spectra in true E_ν at the FD. Matter effects are included in the oscillation probability calculations, with the Earth's crust density assumed to be uniformly 2.84 g/cm³ [78]. Finally, the predicted spectra are converted back to reconstructed E_ν .

To reduce potential bias and the impact of uncertainties from the neutrino interaction model, the extrapolation to predict the disappearance and appearance signals is performed using variables in addition to E_ν . As in the previous analysis, the extrapolation for disappearance is done separately in each reconstructed hadronic energy fraction range (as given in Table I), enabling neutrino interaction processes that occur in different inelasticity regions to be constrained independently. In this analysis, the extrapolation for both disappearance and appearance is additionally performed separately in bins of reconstructed transverse momentum, p_T , of the final state charged lepton. The smaller transverse extent of the ND leads to lower acceptance at higher p_T in the ND

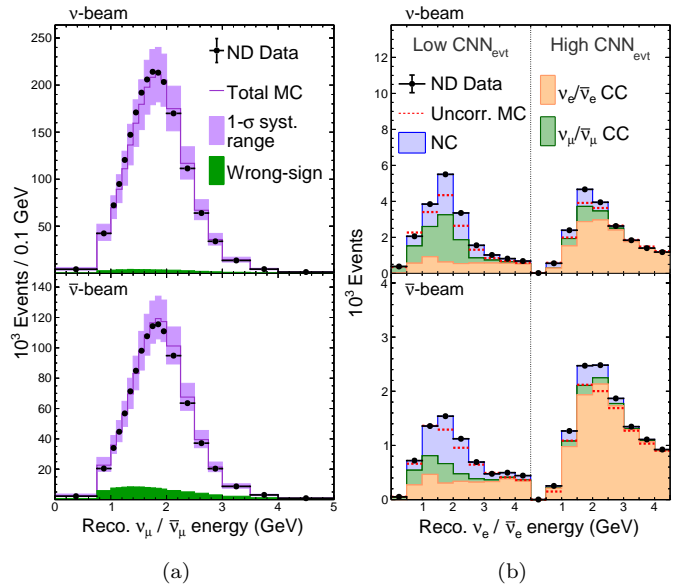


FIG. 1. Reconstructed neutrino energy spectra for the (a) ND ν_μ CC and (b) ND ν_e CC samples with the neutrino-mode beam on top and antineutrino-mode on the bottom [79]. The ν_μ CC E_{frac} sub-samples have been combined. The ν_e CC low and high CNN_{evt} sub-samples are shown. Dashed lines in the ND ν_e and $\bar{\nu}_e$ spectra show the simulated counts before data-driven corrections and the colored regions show the breakdown by interaction type.

than in the FD (Fig. 2), which results in the extrapolated predictions being sensitive to the modeling of the p_T -dependence of the neutrino interactions. Extrapolating in bins of p_T reduces this sensitivity by enabling the ND data to constrain the p_T -dependence. In the ND samples, the p_T bins divide each E_ν bin into three equal populations for the extrapolation, and the resulting FD predictions are summed over the p_T bins for the oscillation fit.

Background spectra at the FD are also predicted using data-driven techniques. Cosmogenic backgrounds in both the appearance and disappearance samples are estimated using FD data collected outside the NuMI beam time window. Beam-induced backgrounds in the appearance samples are primarily CC interactions from the irreducible $\nu_e + \bar{\nu}_e$ component of the beam, with contributions from mis-identified NC and $\nu_\mu + \bar{\nu}_\mu$ CC interactions. Following the procedure from Ref. [1], the FD spectra for these backgrounds are predicted using the spectra of ν_e ($\bar{\nu}_e$) CC candidate events in the ND (Fig. 1b). Misidentified neutrino interactions in the disappearance samples and ν_τ CC interactions in the appearance samples are subdominant backgrounds that are taken directly from the simulations.

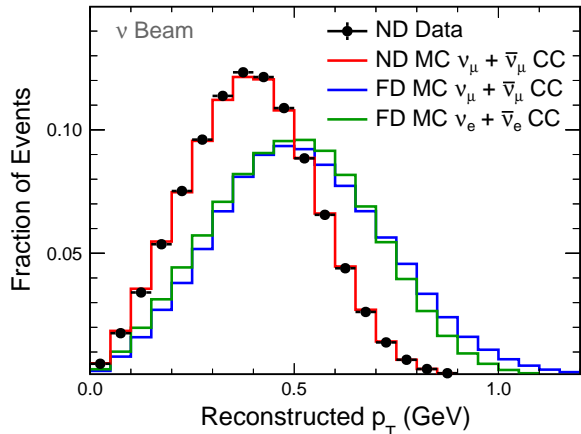


FIG. 2. Distributions from the neutrino-mode beam of the fraction of selected events versus reconstructed p_T of the final state lepton, for the ND ν_μ CC data and simulation, and for the simulated FD ν_μ and ν_e signal events. The corresponding distributions from the antineutrino-mode beam are similar.

V. SYSTEMATIC UNCERTAINTIES

The impacts of systematic uncertainties are evaluated by varying the simulation via event reweighting or simulating alternative event samples and repeating the extrapolation procedure. Uncertainties associated with the neutrino flux, neutron modeling, and detector calibrations are unchanged from the previous analysis [1].

Detector calibration uncertainties remain dominant and are driven by a 5% uncertainty in the calorimetric energy scale. Additionally, a new time-dependent calibration uncertainty is included to account for any residual differences remaining after performing the calibration over shorter time periods as mentioned previously.

Neutrino interaction model uncertainties are evaluated using the event reweighting framework in GENIE with additional uncertainties constructed by NOvA as follows. Uncertainties on CCQE RPA, low- Q^2 RES suppression, 2p2h, and non-resonant and incoherent $N\pi$ production are established for the new model set using methods similar to those in Ref. [80]. Pion FSI uncertainties are based on comparisons to π^+ on ^{12}C scattering data [64–70] and prior studies using an alternative neutrino interaction generator [81]. Uncertainties on the ν_e ($\bar{\nu}_e$) CC cross section relative to the ν_μ ($\bar{\nu}_\mu$) CC cross section due to radiative corrections and possible second-class currents are unchanged from previous analyses [82].

As in the previous analysis, uncertainties are included that are detector specific or account for differences between the ND and FD: the detector masses, beam exposures, kinematic acceptances, beam-induced pile-up, ν_e CC selection in the ND, and cosmogenic backgrounds in the FD. The improved hit clustering algorithm reduces pile-up effects in the ND, decreasing uncertainties for the

associated data-MC selection efficiency differences. An uncertainty for kinematic acceptance differences between the detectors was overestimated in the previous analysis and is subdominant in this analysis after correction. Extrapolating in p_T bins would have substantially reduced the effect of this uncertainty even if left uncorrected.

Uncertainties arising from the custom light model are assigned based on comparison to a more robust response model that was not fully incorporated into the simulation for this analysis. This model is constrained by a sample of ND proton candidates in addition to the muon sample used previously. Differences in the detector response between the proton and muon samples also provide a data-driven uncertainty on the relative production of Cherenkov and scintillation light in the model.

Quantities affected by lepton reconstruction uncertainties include the muon energy scale and lepton angle. The muon energy scale uncertainty now includes a detector mass uncertainty with a component that is uncorrelated between the detectors, plus a correlated component accounting for the Fermi density effect and muon range differences across models. Extrapolating in p_T bins introduces a dependence on the reconstructed lepton angle for which a 10 mrad uncorrelated uncertainty is applied.

Figure 3 shows the impact of the systematic uncertainties on the measurement of $\sin^2 \theta_{23}$, Δm_{32}^2 , and δ_{CP} as evaluated at the determined best-fit point. The extrapolation method significantly reduces the impact of the detector correlated beam flux and neutrino interaction model uncertainties. In contrast, energy calibration and uncorrelated uncertainties that reflect ND-FD differences are less constrained by extrapolation. Figure 3 also shows the impact of uncertainties for extrapolation with and without p_T bins. Extrapolating in p_T bins reduces the interaction model uncertainty by 10-30%, and the total systematic uncertainty by up to 9%. Detector calibration, detector response, and neutron modeling uncertainties that affect the reconstructed energy of the recoiling hadronic system, which is correlated with p_T , are more modestly reduced. The extrapolation in bins of p_T depends on reconstructed lepton kinematics and results in a marginal increase in the associated uncertainties.

VI. RESULTS

The extrapolated predictions of the FD spectra are recomputed for varying oscillation parameters and compared to data using a Poisson negative log-likelihood ratio, $-2 \ln \mathcal{L}$. The best-fit parameters minimize $-2 \ln \mathcal{L}$. The following solar and reactor neutrino experiment constraints are used: $\Delta m_{21}^2 = 7.53 \times 10^{-5} \text{ eV}^2$, $\sin^2 \theta_{12} = 0.307$, and $\sin^2 \theta_{13} = 0.0210 \pm 0.0011$ [83]. The parameters Δm_{32}^2 , $\sin^2 \theta_{23}$, and δ_{CP} are varied without constraints while the 64 systematic uncertainties are assigned penalty terms equal to the square of the number of standard deviations by which they vary from their nominal values. The value of $\sin^2 \theta_{13}$ is allowed to float

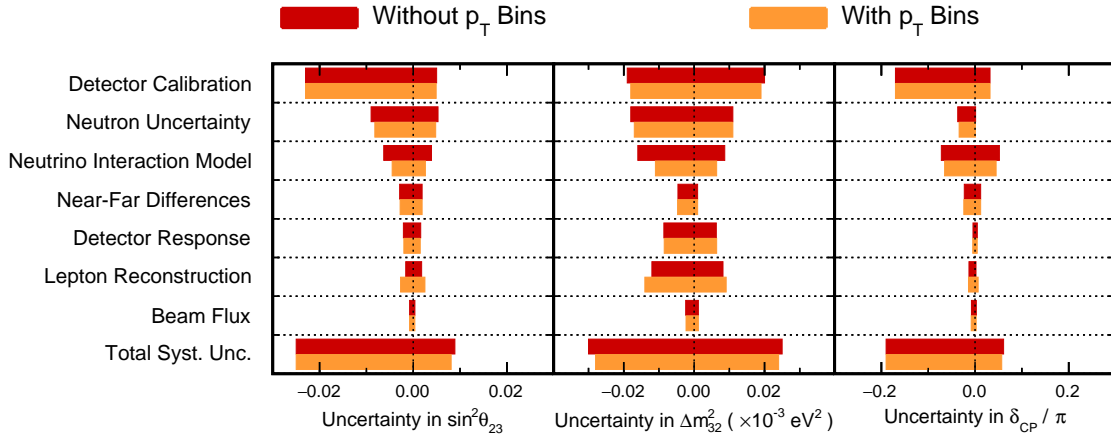


FIG. 3. Systematic uncertainties on $\sin^2 \theta_{23}$, Δm_{32}^2 , and δ_{CP} evaluated at the best-fit point. Detector calibration uncertainties, which are less constrained by extrapolation, are dominant for all three oscillation parameters. Uncertainties for extrapolation with (orange) and without (red) p_T bins are shown for comparison. Extrapolating in p_T bins reduces the total neutrino interaction model uncertainty by 10-30% and the total systematic uncertainty by up to 9%.

similarly. Feldman-Cousins' unified approach [84, 85] is used to determine the confidence intervals for the oscillation parameters.

Figure 4 shows the energy spectra of the ν_μ CC, $\bar{\nu}_\mu$ CC, ν_e CC, and $\bar{\nu}_e$ CC candidates recorded at the FD. The distributions are compared to the oscillation best-fit expectations. Table II summarizes the total event counts and estimated compositions of the selected samples. The CC candidate event samples recorded at the FD include

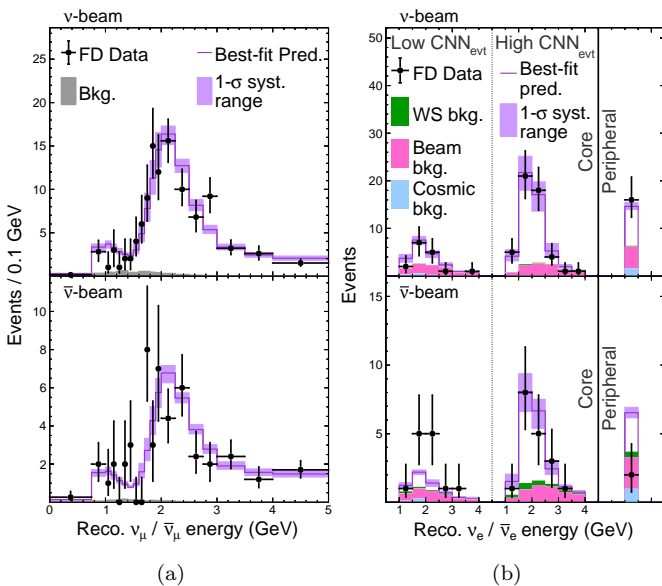


FIG. 4. Reconstructed neutrino energy spectra for the FD (a) ν_μ CC and (b) ν_e CC samples with the neutrino-mode beam on top and antineutrino-mode on the bottom [79]. The ν_μ CC E_{frac} sub-samples have been combined. The ν_e CC low and high CNN_{evt} , and peripheral sub-samples are shown.

211 (105) observed ν_μ ($\bar{\nu}_\mu$) $\rightarrow \nu_\mu$ ($\bar{\nu}_\mu$) events and 82 (33) ν_μ ($\bar{\nu}_\mu$) $\rightarrow \nu_e$ ($\bar{\nu}_e$) candidate events. The latter ν_e ($\bar{\nu}_e$) appearance sample has an estimated background of $26.8^{+1.0}_{-1.3}$ ($14.0^{+0.8}_{-1.1}$).

This analysis determines a best-fit in the normal mass ordering and upper θ_{23} octant (significance of 1.0σ and 1.2σ , respectively), where $-2\ln\mathcal{L} = 173.55$ for 175 degrees of freedom (p-value of 0.705). The data disfavor combinations that lead to a strong asymmetry in the rate of ν_e versus $\bar{\nu}_e$ appearance; therefore, the inverted mass ordering with $\delta_{CP} = \pi/2$ is excluded at more than 3σ and the normal mass ordering with $\delta_{CP} = 3\pi/2$ is disfavored at 2σ confidence. However, owing to the degeneracies, the 90% confidence level allowed regions cover all values of δ_{CP} given permutations of mass ordering and octant. Thus, the current data do not exhibit a preference concerning CP conservation versus violation. Table III shows

TABLE II. Event counts at the FD, both observed and predicted at the best-fit point (see Table III).

	Neutrino beam		Antineutrino beam	
	ν_μ CC	ν_e CC	$\bar{\nu}_\mu$ CC	$\bar{\nu}_e$ CC
$\nu_\mu \rightarrow \nu_\mu$	201.1	1.7	26.0	0.2
$\bar{\nu}_\mu \rightarrow \bar{\nu}_\mu$	12.6	0.0	77.2	0.2
$\nu_\mu \rightarrow \nu_e$	0.1	59.0	0.0	2.3
$\bar{\nu}_\mu \rightarrow \bar{\nu}_e$	0.0	1.0	0.0	19.2
Beam $\nu_e + \bar{\nu}_e$	0.0	14.1	0.0	7.3
NC	2.6	6.3	0.8	2.2
Cosmic	5.0	3.1	0.9	1.6
Others	0.9	0.5	0.4	0.3
Signal	$214.1^{+14.4}_{-14.0}$	$59.0^{+2.5}_{-2.5}$	$103.4^{+7.1}_{-7.0}$	$19.2^{+0.6}_{-0.7}$
Background	$8.2^{+1.9}_{-1.7}$	$26.8^{+1.6}_{-1.7}$	$2.1^{+0.7}_{-0.7}$	$14.0^{+0.9}_{-1.0}$
Best fit	222.3	85.8	105.4	33.2
Observed	211	82	105	33

TABLE III. Summary of oscillation parameter best-fit results for different choices of the mass ordering (Normal or Inverted) and upper or lower θ_{23} octant (UO, LO), along with the significance (in units of σ) at which those combinations are disfavored.

Parameter	Normal ord.		Inverted ord.	
	UO	LO	UO	LO
$\Delta m_{32}^2 (10^{-3} \text{ eV}^2)$	$+2.41 \pm 0.07$	$+2.39$	-2.45	-2.44
$\sin^2 \theta_{23}$	$0.57^{+0.03}_{-0.04}$	0.46	0.56	0.46
$\delta_{\text{CP}} (\pi)$	$0.82^{+0.27}_{-0.87}$	0.07	1.52	1.41
Rejection significance	-	1.1σ	0.9σ	1.1σ

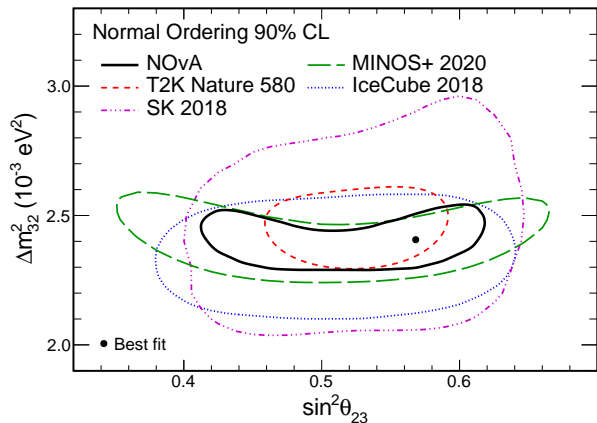


FIG. 5. The 90% confidence level region for Δm_{32}^2 and $\sin^2 \theta_{23}$, with the NOvA allowed region and best-fit point [86] superposed on contours from other experiments. [87–90]².

the best-fit parameter values for each choice of θ_{23} octant and mass ordering.

Figure 5 compares the 90% confidence level contours for Δm_{32}^2 and $\sin^2 \theta_{23}$ with those of other experiments [87–90]². Allowed regions in $\sin^2 \theta_{23}$ and δ_{CP} are shown in Fig. 6 and are compared with a recent best fit from T2K [87]².

As shown in Fig. 6a, the T2K best-fit point is in the NO but lies in a region that NOvA disfavors. However, some regions of overlap remain. Figure 6b shows that for IO, the T2K allowed region at 90% confidence level is entirely contained within the corresponding NOvA allowed region. This outcome reflects in part the circumstance that T2K observes a relatively more pronounced asymmetry in ν_e versus $\bar{\nu}_e$ oscillations.

Although each experiment reports a mild preference for NO, it has been suggested that a joint fit of the two experiments might converge on an IO solution [93]. Some

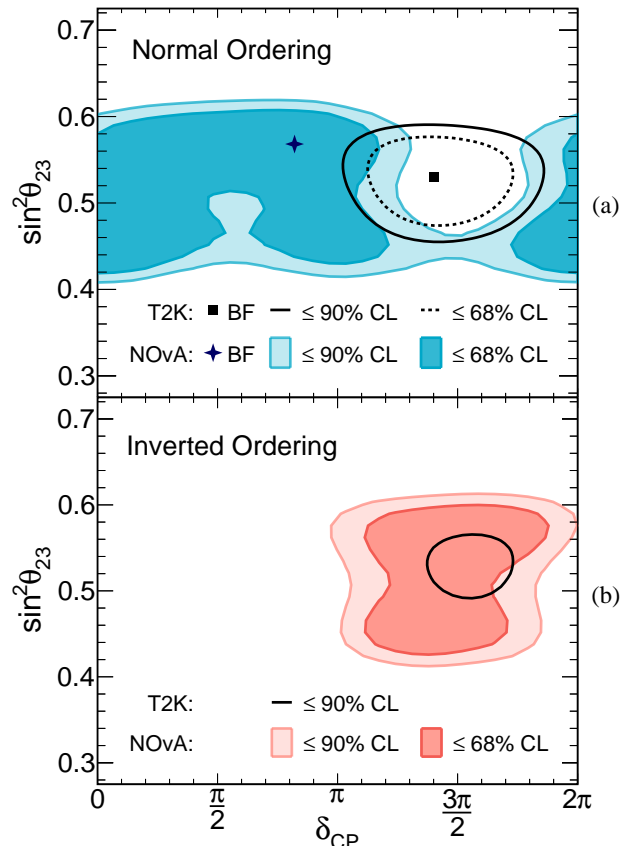


FIG. 6. The 68% and 90% confidence level contours in $\sin^2 \theta_{23}$ vs. δ_{CP} in the (a) normal mass ordering and (b) inverted mass ordering [91]. The cross denotes the NOvA best-fit point and colored areas depict the 90% and 68% allowed regions. Overlaid black solid-line and dashed-line contours depict allowed regions reported by T2K [87]².

authors have also explored the possibility that the differences in the $\nu_\mu \rightarrow \nu_e$ and $\bar{\nu}_\mu \rightarrow \bar{\nu}_e$ rates seen by the experiments are explained by additional non-standard matter effects [94, 95].

In conclusion, we have presented improved measurements of oscillation parameters Δm_{32}^2 , $\sin^2 \theta_{23}$, and δ_{CP} , including an expanded data set and enhanced analysis techniques with respect to previous publications. These measurements continue to favor the normal mass ordering and upper octant of $\sin^2 \theta_{23}$, as well as values of the oscillation parameters that do not lead to a large asymmetry in $\nu_\mu \rightarrow \nu_e$ and $\bar{\nu}_\mu \rightarrow \bar{\nu}_e$ oscillation rates.

VII. ACKNOWLEDGMENTS

This document was prepared by the NOvA collaboration using the resources of the Fermi National Accelerator Laboratory (Fermilab), a U.S. Department of Energy, Office of Science, HEP User Facility. Fermilab is man-

² While this paper was in its final internal review, an updated analysis was published by the T2K collaboration [92]. In Ref. [92] the dataset remains unchanged and the same approach is used. The conclusions drawn from the comparisons of the contours remains unchanged.

aged by Fermi Research Alliance, LLC (FRA), acting under Contract No. DE-AC02-07CH11359. This work was supported by the U.S. Department of Energy; the U.S. National Science Foundation; the Department of Science and Technology, India; the European Research Council; the MSMT CR, GA UK, Czech Republic; the

RAS, RFBR, RMES, RSF, and BASIS Foundation, Russia; CNPq and FAPEG, Brazil; STFC, UKRI, and the Royal Society, United Kingdom; and the State and University of Minnesota. We are grateful for the contributions of the staffs of the University of Minnesota at the Ash River Laboratory and of Fermilab.

-
- [1] M. A. Acero *et al.* (NOvA), First Measurement of Neutrino Oscillation Parameters using Neutrinos and Antineutrinos by NOvA, *Phys. Rev. Lett.* **123**, 151803 (2019), arXiv:1906.04907 [hep-ex].
- [2] Y. Fukuda *et al.* (Super-Kamiokande), Evidence for oscillation of atmospheric neutrinos, *Phys. Rev. Lett.* **81**, 1562 (1998), arXiv:hep-ex/9807003 [hep-ex].
- [3] S. Fukuda *et al.* (Super-Kamiokande), Determination of solar neutrino oscillation parameters using 1496 days of Super-Kamiokande I data, *Phys. Lett. B* **539**, 179 (2002), arXiv:hep-ex/0205075 [hep-ex].
- [4] Q. R. Ahmad *et al.* (SNO), Direct evidence for neutrino flavor transformation from neutral current interactions in the Sudbury Neutrino Observatory, *Phys. Rev. Lett.* **89**, 011301 (2002), arXiv:nucl-ex/0204008 [nucl-ex].
- [5] K. Eguchi *et al.* (KamLAND), First results from KamLAND: Evidence for reactor anti-neutrino disappearance, *Phys. Rev. Lett.* **90**, 021802 (2003), arXiv:hep-ex/0212021 [hep-ex].
- [6] D. G. Michael *et al.* (MINOS), Observation of muon neutrino disappearance with the MINOS detectors and the NuMI neutrino beam, *Phys. Rev. Lett.* **97**, 191801 (2006), arXiv:hep-ex/0607088 [hep-ex].
- [7] K. Abe *et al.* (T2K), Indication of Electron Neutrino Appearance from an Accelerator-produced Off-axis Muon Neutrino Beam, *Phys. Rev. Lett.* **107**, 041801 (2011), arXiv:1106.2822 [hep-ex].
- [8] Y. Abe *et al.* (Double Chooz), Indication of Reactor $\bar{\nu}_e$ Disappearance in the Double Chooz Experiment, *Phys. Rev. Lett.* **108**, 131801 (2012), arXiv:1112.6353 [hep-ex].
- [9] F. P. An *et al.* (Daya Bay), Observation of electron-antineutrino disappearance at Daya Bay, *Phys. Rev. Lett.* **108**, 171803 (2012), arXiv:1203.1669 [hep-ex].
- [10] J. K. Ahn *et al.* (RENO), Observation of Reactor Electron Antineutrino Disappearance in the RENO Experiment, *Phys. Rev. Lett.* **108**, 191802 (2012), arXiv:1204.0626 [hep-ex].
- [11] R. N. Mohapatra and A. Y. Smirnov, Neutrino Mass and New Physics, *Elementary particle physics. Proceedings, Corfu Summer Institute, CORFU2005, Corfu, Greece, September 4-26, 2005*, *Ann. Rev. Nucl. Part. Sci.* **56**, 569 (2006), arXiv:hep-ph/0603118 [hep-ph].
- [12] H. Nunokawa, S. J. Parke, and J. W. F. Valle, CP Violation and Neutrino Oscillations, *Prog. Part. Nucl. Phys.* **60**, 338 (2008), arXiv:0710.0554 [hep-ph].
- [13] G. Altarelli and F. Feruglio, Discrete Flavor Symmetries and Models of Neutrino Mixing, *Rev. Mod. Phys.* **82**, 2701 (2010), arXiv:1002.0211 [hep-ph].
- [14] S. F. King, Models of Neutrino Mass, Mixing and CP Violation, *J. Phys. G* **42**, 123001 (2015), arXiv:1510.02091 [hep-ph].
- [15] S. T. Petcov, Discrete Flavour Symmetries, Neutrino Mixing and Leptonic CP Violation, *Eur. Phys. J. C* **78**, 709 (2018), arXiv:1711.10806 [hep-ph].
- [16] S. Pascoli and S. T. Petcov, The SNO solar neutrino data, neutrinoless double beta decay and neutrino mass spectrum, *Phys. Lett. B* **544**, 239 (2002), arXiv:hep-ph/0205022 [hep-ph].
- [17] J. N. Bahcall, H. Murayama, and C. Pena-Garay, What can we learn from neutrinoless double beta decay experiments?, *Phys. Rev. D* **70**, 033012 (2004), arXiv:hep-ph/0403167 [hep-ph].
- [18] L. Wolfenstein, Neutrino Oscillations in Matter, *Phys. Rev. D* **17**, 2369 (1978).
- [19] P. F. Harrison and W. G. Scott, mu - tau reflection symmetry in lepton mixing and neutrino oscillations, *Phys. Lett. B* **547**, 219 (2002), arXiv:hep-ph/0210197.
- [20] M. Fukugita and T. Yanagida, Baryogenesis Without Grand Unification, *Phys. Lett. B* **174**, 45 (1986).
- [21] W. Buchmuller and M. Plumacher, Baryon asymmetry and neutrino mixing, *Phys. Lett. B* **389**, 73 (1996), arXiv:hep-ph/9608308.
- [22] W. Buchmuller, P. Di Bari, and M. Plumacher, Leptogenesis for pedestrians, *Annals Phys.* **315**, 305 (2005), arXiv:hep-ph/0401240.
- [23] W. Buchmuller, R. D. Peccei, and T. Yanagida, Leptogenesis as the origin of matter, *Ann. Rev. Nucl. Part. Sci.* **55**, 311 (2005), arXiv:hep-ph/0502169.
- [24] A. Pilaftsis, CP violation and baryogenesis due to heavy Majorana neutrinos, *Phys. Rev. D* **56**, 5431 (1997), arXiv:hep-ph/9707235.
- [25] D. S. Ayres *et al.* (NOvA), The NOvA Technical Design Report (2007).
- [26] P. Adamson *et al.*, The NuMI Neutrino Beam, *Nucl. Instrum. Meth. A* **806**, 279 (2016), arXiv:1507.06690 [physics.acc-ph].
- [27] S. Mufson *et al.*, Liquid scintillator production for the NOvA experiment, *Nucl. Instrum. Meth. A* **799**, 1 (2015), arXiv:1504.04035 [physics.ins-det].
- [28] S. Agostinelli *et al.* (GEANT4), GEANT4—a simulation toolkit, *Nucl. Instrum. Meth. A* **506**, 250 (2003).
- [29] L. Aliaga *et al.* (MINERvA), Neutrino Flux Predictions for the NuMI Beam, *Phys. Rev. D* **94**, 092005 (2016), [Addendum: *Phys. Rev. D* **95**, no.3, 039903 (2017)], arXiv:1607.00704 [hep-ex].
- [30] J. M. Paley *et al.* (MIPP), Measurement of Charged Pion Production Yields off the NuMI Target, *Phys. Rev. D* **90**, 032001 (2014), arXiv:1404.5882 [hep-ex].
- [31] C. Alt *et al.* (NA49), Inclusive production of charged pions in p+C collisions at 158-GeV/c beam momentum, *Eur. Phys. J. C* **49**, 897 (2007), arXiv:hep-ex/0606028 [hep-ex].
- [32] N. Abgrall *et al.* (NA61/SHINE), Measurements of Cross Sections and Charged Pion Spectra in Proton-Carbon Interactions at 31 GeV/c, *Phys. Rev. C* **84**, 034604 (2011), arXiv:1102.0983 [hep-ex].

- [33] D. S. Barton *et al.*, Experimental Study of the α -Dependence of Inclusive Hadron Fragmentation, *Phys. Rev. D* **27**, 2580 (1983).
- [34] S. M. Seun, *Measurement of $\pi - K$ ratios from the NuMI target*, Ph.D. thesis, Harvard U. (2007).
- [35] G. M. Tinti, *Sterile neutrino oscillations in MINOS and hadron production in pC collisions*, Ph.D. thesis, Oxford U. (2010).
- [36] A. V. Lebedev, *Ratio of pion kaon production in proton carbon interactions*, Ph.D. thesis, Harvard U. (2007).
- [37] B. Baatar *et al.* (NA49), Inclusive production of protons, anti-protons, neutrons, deuterons and tritons in p+C collisions at 158 GeV/c beam momentum, *Eur. Phys. J. C* **73**, 2364 (2013), arXiv:1207.6520 [hep-ex].
- [38] P. Skubic *et al.*, Neutral Strange Particle Production by 300-GeV Protons, *Phys. Rev. D* **18**, 3115 (1978).
- [39] S. P. Denisov, S. V. Donskov, Yu. P. Gorin, R. N. Krasnokutsky, A. I. Petrukhin, Yu. D. Prokoshkin, and D. A. Stoyanova, Absorption cross-sections for pions, kaons, protons and anti-protons on complex nuclei in the 6-GeV/c to 60-GeV/c momentum range, *Nucl. Phys. B* **61**, 62 (1973).
- [40] A. S. Carroll *et al.*, Absorption Cross-Sections of π^\pm , K^\pm , p and \bar{p} on Nuclei Between 60 GeV/c and 280 GeV/c, *Phys. Lett. B* **80**, 319 (1979).
- [41] K. Abe *et al.* (T2K), T2K neutrino flux prediction, *Phys. Rev. D* **87**, 012001 (2013), [Addendum: *Phys. Rev. D* **87**, no.1, 019902(2013)], arXiv:1211.0469 [hep-ex].
- [42] T. K. Gaisser, G. B. Yodh, V. D. Barger, and F. Halzen, On the Relation Between Proton-Proton and Proton-Nucleus Cross-Sections at Very High-Energies, in *14th International Cosmic Ray Conference (ICRC 1975) Munich, Germany, August 15-29, 1975* (1975) pp. 2161–2166.
- [43] J. W. Cronin, R. Cool, and A. Abashian, Cross Sections of Nuclei for High-Energy Pions, *Phys. Rev.* **107**, 1121 (1957).
- [44] J. V. Allaby *et al.* (IHEP-CERN), Total cross-sections of pi-minus, k-minus, and anti-p on protons and deuterons in the momentum range 20-65 GeV/c, *Phys. Lett.* **30B**, 500 (1969).
- [45] M. J. Longo and B. J. Moyer, Nucleon and Nuclear Cross Sections for Positive Pions and Protons above 1.4 BeV/c, *Phys. Rev.* **125**, 701 (1962).
- [46] B. M. Bobchenko *et al.*, Measurement of total inelastic cross-sections from proton interactions with Nuclei in the momentum range from 5 GeV/c to 9 GeV/c and pi mesons from with nuclei in the momentum range from 1.75 GeV/c to 6.5 GeV/c, *Sov. J. Nucl. Phys.* **30**, 805 (1979), [*Yad. Fiz.* **30**, 1553(1979)].
- [47] V. B. Fedorov, Yu. G. Grishuk, M. V. Kosov, G. A. Leksin, N. A. Pivnyuk, S. V. Shevchenko, V. L. Stolin, A. V. Vlasov, and L. S. Vorobev, Total Inelastic Cross-Sections for pi Mesons on Nuclei in the 2-GeV/c to 6-GeV/c Momentum Range, *Sov. J. Nucl. Phys.* **27**, 222 (1978), [*Yad. Fiz.* **27**, 413(1978)].
- [48] R. J. Abrams, R. L. Cool, G. Giacomelli, T. F. Kycia, B. A. Leontic, K. K. Li, and D. N. Michael, Total cross-sections of K \pm mesons and anti-protons on nucleons up to 3.3-GeV/c, *Phys. Rev. D* **1**, 1917 (1970).
- [49] C. Andreopoulos *et al.*, The GENIE Neutrino Monte Carlo Generator, *Nucl. Instrum. Meth. A* **614**, 87 (2010), arXiv:0905.2517 [hep-ph].
- [50] C. Andreopoulos, C. Barry, S. Dytman, H. Gallagher, T. Golan, R. Hatcher, G. Perdue, and J. Yarba, The GENIE Neutrino Monte Carlo Generator: Physics and User Manual (2015), arXiv:1510.05494 [hep-ph].
- [51] J. Nieves, J. E. Amaro, and M. Valverde, Inclusive quasi-elastic neutrino reactions, *Phys. Rev. C* **70**, 055503 (2004), [Erratum: *Phys. Rev. C* **72**, 019902(2005)], arXiv:nucl-th/0408005 [nucl-th].
- [52] R. Gran, J. Nieves, F. Sanchez, and M. J. Vicente Vacas, Neutrino-nucleus quasi-elastic and 2p2h interactions up to 10 GeV, *Phys. Rev. D* **88**, 113007 (2013), arXiv:1307.8105 [hep-ph].
- [53] M. Martini, M. Ericson, G. Chanfray, and J. Marteau, A Unified approach for nucleon knock-out, coherent and incoherent pion production in neutrino interactions with nuclei, *Phys. Rev. C* **80**, 065501 (2009), arXiv:0910.2622 [nucl-th].
- [54] V. Pandey, N. Jachowicz, T. Van Cuyck, J. Ryckebusch, and M. Martini, Low-energy excitations and quasielastic contribution to electron-nucleus and neutrino-nucleus scattering in the continuum random-phase approximation, *Phys. Rev. C* **92**, 024606 (2015), arXiv:1412.4624 [nucl-th].
- [55] A. S. Meyer, M. Betancourt, R. Gran, and R. J. Hill, Deuterium target data for precision neutrino-nucleus cross sections, *Phys. Rev. D* **93**, 113015 (2016), arXiv:1603.03048 [hep-ph].
- [56] A. Bodek and J. L. Ritchie, Further Studies of Fermi Motion Effects in Lepton Scattering from Nuclear Targets, *Phys. Rev. D* **24**, 1400 (1981).
- [57] C. Berger and L. M. Sehgal, Lepton mass effects in single pion production by neutrinos, *Phys. Rev. D* **76**, 113004 (2007), arXiv:0709.4378 [hep-ph].
- [58] C. Berger and L. M. Sehgal, PCAC and coherent pion production by low energy neutrinos, *Phys. Rev. D* **79**, 053003 (2009), arXiv:0812.2653 [hep-ph].
- [59] A. Bodek and U. K. Yang, Higher twist, xi(omega) scaling, and effective LO PDFs for lepton scattering in the few GeV region, *Neutrino factories. Proceedings, 4th International Workshop, NuFact'02, London, UK, July 1-6, 2002*, *J. Phys. G* **29**, 1899 (2003), arXiv:hep-ex/0210024 [hep-ex].
- [60] T. Yang, C. Andreopoulos, H. Gallagher, K. Hoffmann, and P. Kehayias, A Hadronization Model for Few-GeV Neutrino Interactions, *Eur. Phys. J. C* **63**, 1 (2009), arXiv:0904.4043 [hep-ph].
- [61] T. Sjostrand, S. Mrenna, and P. Z. Skands, PYTHIA 6.4 Physics and Manual, *JHEP* **05**, 026, arXiv:hep-ph/0603175 [hep-ph].
- [62] L. L. Salcedo, E. Oset, M. J. Vicente-Vacas, and C. Garcia-Recio, Computer Simulation of Inclusive Pion Nuclear Reactions, *Nucl. Phys. A* **484**, 557 (1988).
- [63] R. Gran *et al.* (MINERvA), Antineutrino Charged-Current Reactions on Hydrocarbon with Low Momentum Transfer, *Phys. Rev. Lett.* **120**, 221805 (2018), arXiv:1803.09377 [hep-ex].
- [64] B. W. Allardyce *et al.*, Pion reaction cross-sections and nuclear sizes, *Nucl. Phys. A* **209**, 1 (1973).
- [65] A. Saunders, S. Hoeibraten, J. J. Kraushaar, B. J. Kriss, R. J. Peterson, R. A. Ristinen, J. T. Brack, G. Hofman, E. F. Gibson, and C. L. Morris, Reaction and total cross-sections for low-energy pi $^+$ and pi $^-$ on isospin zero nuclei, *Phys. Rev. C* **53**, 1745 (1996).

- [66] O. Meirav, E. Friedman, R. R. Johnson, R. Olszewski, and P. Weber, Low-energy Pion - Nucleus Potentials From Differential and Integral Data, *Phys. Rev. C* **40**, 843 (1989).
- [67] S. M. Levenson *et al.*, Inclusive pion scattering in the delta (1232) region, *Phys. Rev. C* **28**, 326 (1983).
- [68] D. Ashery, I. Navon, G. Azuelos, H. K. Walter, H. J. Pfeiffer, and F. W. Schlepütz, True Absorption and Scattering of Pions on Nuclei, *Phys. Rev. C* **23**, 2173 (1981).
- [69] D. Ashery *et al.*, Inclusive pion single charge exchange reactions, *Phys. Rev. C* **30**, 946 (1984).
- [70] E. S. Pinzon Guerra *et al.* (DUET), Measurement of σ_{ABS} and σ_{CX} of π^+ on carbon by the Dual Use Experiment at TRIUMF (DUET), *Phys. Rev. C* **95**, 045203 (2017), arXiv:1611.05612 [hep-ex].
- [71] Geant4 Collaboration, Geant4 10.4 Release Notes, <https://geant4-data.web.cern.ch/ReleaseNotes/ReleaseNotes4.10.4.html> (2017).
- [72] A. Aurisano, C. Backhouse, R. Hatcher, N. Mayer, J. Musser, R. Patterson, R. Schroeter, and A. Sousa (NOvA), The NOvA simulation chain, *Proceedings, 21st International Conference on Computing in High Energy and Nuclear Physics (CHEP 2015): Okinawa, Japan, April 13-17, 2015*, *J. Phys. Conf. Ser.* **664**, 072002 (2015).
- [73] R. M. Sternheimer, The Density Effect for Ionization Loss in Materials, *Phys. Rev.* **88**, 851 (1952).
- [74] D. S. Pershey, *A Measurement of ν_e Appearance and ν_μ Disappearance Neutrino Oscillations with the NOvA Experiment*, Ph.D. thesis, Caltech (2018).
- [75] A. Aurisano, A. Radovic, D. Rocco, A. Himmel, M. D. Messier, E. Niner, G. Pawloski, F. Psihas, A. Sousa, and P. Vahle, A Convolutional Neural Network Neutrino Event Classifier, *JINST* **11** (09), P09001, arXiv:1604.01444 [hep-ex].
- [76] M. Groh, *Constraints on Neutrino Oscillation Parameters from Neutrinos and Antineutrinos with Machine Learning*, Ph.D. thesis, Indiana U., Bloomington (main) (2021).
- [77] F. Psihas, *Measurement of Long Baseline Neutrino Oscillations and Improvements from Deep Learning*, Ph.D. thesis, Indiana U. (2018).
- [78] C. Bassin, G. Laske, and G. Masters, The current limits of resolution for surface wave tomography in North America. *eos trans agu 81:f897*, *EOS Trans AGU* **81**, F897 (2000).
- [79] See Supplemental Material at [[To be inserted by publisher] for the muon neutrino distributions in each quartile of hadronic energy fraction (2021).
- [80] M. A. Acero *et al.* (NOvA), Adjusting neutrino interaction models and evaluating uncertainties using NOvA near detector data, *Eur. Phys. J. C* **80**, 1119 (2020), arXiv:2006.08727 [hep-ex].
- [81] E. S. Pinzon Guerra *et al.*, Using world charged π^\pm -nucleus scattering data to constrain an intranuclear cascade model, *Phys. Rev. D* **99**, 052007 (2019), arXiv:1812.06912 [hep-ex].
- [82] M. A. Acero *et al.* (NOvA), New constraints on oscillation parameters from ν_e appearance and ν_μ disappearance in the NOvA experiment, *Phys. Rev. D* **98**, 032012 (2018), arXiv:1806.00096 [hep-ex].
- [83] M. Tanabashi *et al.* (Particle Data Group), Review of particle physics, *Phys. Rev. D* **98**, 030001 (2018 and the 2019 update).
- [84] G. J. Feldman and R. D. Cousins, A Unified approach to the classical statistical analysis of small signals, *Phys. Rev. D* **57**, 3873 (1998), arXiv:physics/9711021 [physics.data-an].
- [85] A. Sousa, N. Buchanan, S. Calvez, P. Ding, D. Doyle, A. Himmel, B. Holzman, J. Kowalkowski, A. Norman, and T. Peterka, Implementation of Feldman-Cousins Corrections and Oscillation Calculations in the HPC Environment for the NOvA Experiment, *EPJ Web Conf.* **214**, 05012 (2019).
- [86] See Supplemental Material at [to be inserted by publisher] for the profiles of these surfaces on the Δm_{32}^2 and $\sin^2 \theta_{23}$ axes as well as the surfaces computed for the inverted hierarchy case (2021).
- [87] K. Abe *et al.* (T2K), Constraint on the matter-antimatter symmetry-violating phase in neutrino oscillations, *Nature* **580**, 339 (2020), [Erratum: *Nature* 583, E16 (2020)], arXiv:1910.03887 [hep-ex].
- [88] K. Abe *et al.* (Super-Kamiokande), Atmospheric neutrino oscillation analysis with external constraints in Super-Kamiokande I-IV, *Phys. Rev. D* **97**, 072001 (2018), arXiv:1710.09126 [hep-ex].
- [89] P. Adamson *et al.* (MINOS+), Precision Constraints for Three-Flavor Neutrino Oscillations from the Full MINOS+ and MINOS Dataset, *Phys. Rev. Lett.* **125**, 131802 (2020), arXiv:2006.15208 [hep-ex].
- [90] M. G. Aartsen *et al.* (IceCube), Measurement of Atmospheric Neutrino Oscillations at 6–56 GeV with IceCube DeepCore, *Phys. Rev. Lett.* **120**, 071801 (2018), arXiv:1707.07081 [hep-ex].
- [91] See Supplemental Material at [To be inserted by publisher] for profiles of these surfaces on the δ_{CP} axis (2021).
- [92] K. Abe *et al.* (T2K), Improved constraints on neutrino mixing from the T2K experiment with 3.13×10^{21} protons on target, *Phys. Rev. D* **103**, 112008 (2021), arXiv:2101.03779 [hep-ex].
- [93] K. J. Kelly, P. A. Machado, S. J. Parke, Y. F. Perez Gonzalez, and R. Zukanovich-Funchal, Back to (Mass-)Square(d) One: The Neutrino Mass Ordering in Light of Recent Data, *Phys. Rev. D* **103**, 013004 (2021), arXiv:2007.08526 [hep-ph].
- [94] P. B. Denton, J. Gehrlein, and R. Pestes, *CP* -Violating Neutrino Nonstandard Interactions in Long-Baseline-Accelerator Data, *Phys. Rev. Lett.* **126**, 051801 (2021), arXiv:2008.01110 [hep-ph].
- [95] S. S. Chatterjee and A. Palazzo, Non-standard neutrino interactions as a solution to the NOvA and T2K discrepancy, *Phys. Rev. Lett.* **126**, 051802 (2021), arXiv:2008.04161 [hep-ph].